Solid State Nuclear Magnetic Resonance 87 (2017) 54–64

Contents lists available at ScienceDirect

Solid State Nuclear Magnetic Resonance

journal homepage: www.elsevier.com/locate/ssnmr

Investigation of zeolitic imidazolate frameworks using ^{13}C and ^{15}N solid-state NMR spectroscopy

Scott Sneddon, Jürgen Kahr, Angelica F. Orsi, David J. Price, Daniel M. Dawson, Paul A. Wright, Sharon E. Ashbrook *

School of Chemistry, EaStCHEM and Centre of Magnetic Resonance, University of St Andrews, St Andrews KY16 9ST, United Kingdom

ARTICLE INFO

Keywords:
Zeolitic imidazolate frameworks
Microporous materials
ZIFs
DFT
Solid-state NMR
^{13}C NMR
^{15}N NMR
CSA-amplified PASS

ABSTRACT

Zeolitic imidazolate frameworks (ZIFs) are a subclass of metal-organic frameworks (MOFs) with extended three-dimensional networks of transition metal nodes (bridged by rigid imidazolate linkers), with potential applications in gas storage and separation, sensing and controlled delivery of drug molecules. Here, we investigate the use of ^{13}C and ^{15}N solid-state NMR spectroscopy to characterise the local structure and disorder in a variety of single- and dual-linker ZIFs. In most cases, a combination of a basic knowledge of chemical shifts typically observed in solution-state NMR spectroscopy and the use of dipolar dephasing NMR experiments to reveal information about quaternary carbon species are combined to enable spectral assignment. Accurate measurement of the anisotropic components of the chemical shift provided additional information to characterise the local environment and the possibility of trying to understand the relationships between NMR parameters and both local and long-range structure. First-principles calculations on some of the simpler, ordered ZIFs were possible, and provided support for the spectral assignments, while comparison of these model systems to more disordered ZIFs aided interpretation of the more complex spectra obtained. It is shown that ^{13}C and ^{15}N NMR are sufficiently sensitive to detect small changes in the local environment, *e.g.*, functionalisation of the linker, crystallographic inequivalence and changes to the framework topology, while the relative proportion of each linker present can be obtained by comparing relative intensities of resonances corresponding to chemically-similar species in cross polarisation experiments with short contact times. Therefore, multinuclear NMR spectroscopy, and in particular the measurement of both isotropic and anisotropic parameters, offers a useful tool for the structural study of ordered and, in particular, disordered ZIFs.

1. Introduction

Zeolitic imidazolate frameworks (ZIFs) are a relatively new subclass of metal-organic frameworks (MOFs) with extended three-dimensional networks of transition metal nodes (predominantly Zn^{2+} or Co^{2+}) bridged by rigid imidazolate linkers [1,2]. The observed Zn-Im-Zn bond angles are similar to that of the ideal Si—O—Si bond angle (~145°) found in zeolites, so that many ZIFs exhibit the same framework topologies as zeolites, although ZIFs with unique framework topologies have also been synthesised [2]. As an example, Fig. 1a shows the structure of ZIF-65, which is synthesised with 2-nitroimidazolate as the linker, and exhibits the well-known sodalite (SOD) framework topology [3]. ZIFs have attracted considerable recent attention, owing to their potential applications in gas storage and separation, fluid separation, sensing, encapsulation and controlled delivery of drug molecules [2,4–9]. The range of applications can be widened by using functionalised imidazolate linkers, altering the chemical nature of the pores produced, while maintaining the framework topology [10]. Additionally, more than one type of imidazolate linker can be included into the framework structure [2].

ZIFs are typically synthesised by reacting a hydrated transition metal salt (*e.g.*, $Zn(NO_2)_2{\cdot}6H_2O$) with the desired imidazole (or functionalised imidazole) in a polar amide solvent (*e.g.*, *N,N*-dimethylformamide (DMF)). In their as-prepared forms, many ZIFs contain solvent molecules in the pores, which can usually be removed by exchange or heating [1]. The linker/metal ratio and the concentration of the metal ion in solution are important factors for achieving the desired final product, and it has been shown that by varying these it is possible to target specific framework topologies [2]. As described above, a range of linkers can be used to prepare ZIFs – those used in this work are given (along with the naming

* Corresponding author.
E-mail address: sema@st-andrews.ac.uk (S.E. Ashbrook).

http://dx.doi.org/10.1016/j.ssnmr.2017.09.001
Received 8 August 2017; Received in revised form 4 September 2017; Accepted 5 September 2017
Available online 9 September 2017

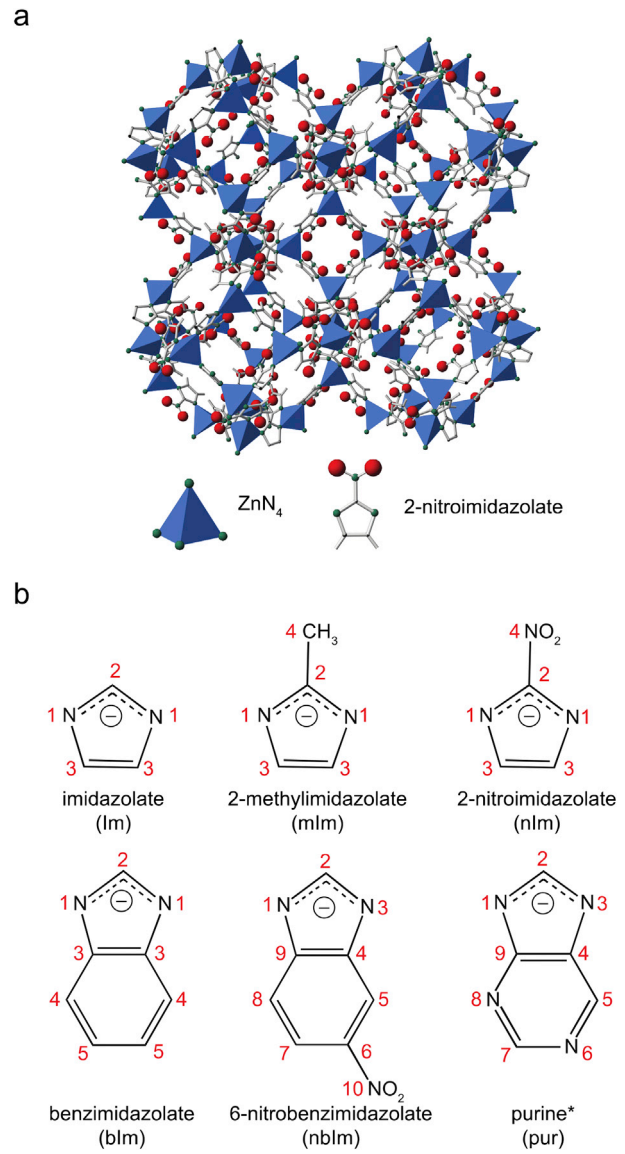

Fig. 1. (a) Structure of ZIF-65 (which contains a 2-nitroimidazolate (nIm) linker and Zn^{2+} cations). (b) Chemical structure, nomenclature and numbering schemes for the imidazolate used in this work. Note that the numbering scheme used for pur is not that typically used in organic chemistry, but has been chosen to facilitate comparison with other linkers.

and numbering conventions used) in Fig. 1b, and the ZIFs synthesised from them outlined in Table 1. (Note that the numbering scheme used for the purine (pur) linker is not that used conventionally in organic chemistry, but has been chosen to facilitate comparison with other linkers). It has been shown that linkers with "bulkier" functional groups, such as benzimidazolate (bIm), produce framework materials with larger pores and/or windows, whereas linkers with smaller functional groups, such as 2-nitroimidazolate (nIm), typically produce smaller pores with narrower apertures [2,11]. Using a combination of more than one type of linker, more complex structural frameworks, which exhibit a wider range of chemical or physical properties, can be synthesised. For example, ZIF-68 (GME topology), which is synthesised with 2-nitroimidazolate and benzimidazolate (in a 1:1 ratio), has both hydrophilic and hydrophobic pores [11]. There are a few examples of ZIFs that have been prepared with more than one metal centre [12–14], which can result in a material that possesses different metal coordination environments, with a unique chemistry that can be exploited for various applications, such as catalysis.

Table 1
The linker(s) used, the framework topology adopted and the corresponding CCDC code for ZIFs synthesised in this work.

ZIF	Reference	Topology	Linker(s)	CCDC code
ZIF-7	[35]	SOD	bIm	VELVIS
ZIF-8	[35]	SOD	mIm	VELVOY
ZIF-11	[1]	RHO	bIm	VEJZOA
ZIF-20	[36]	LTA	pur	MIHHAN
ZIF-65	[3]	SOD	nIm	GITTIN
ZIF-68	[3]	GME	nIm + bIm	GITTUZ
ZIF-70	[3]	GME	Im + nIm	GITVEL
ZIF-78	[11]	GME	nIm + nbIm	YOZBIZ

The characterisation of ZIFs commonly uses diffraction-based experiments, such as single-crystal or powder X-ray diffraction (XRD). Such experiments are able to provide the average (over both time and space) positions of the atoms in an average unit cell. Although single-crystal diffraction is an extremely powerful technique for structure solution, this approach is limited by the need for a suitably large and stable single crystal. Solving structures from powder XRD data is much more challenging, particularly if the sample is poorly crystalline, owing to the presence of fewer resolved reflections in the diffraction pattern. Difficulties can also occur in refinements when lighter atoms, such as C, N and H, or isoelectronic species, are present in the material. Furthermore, if there is any disorder present, be it compositional (resulting from the use of more than one type of linker/metal in the synthesis), positional (arising from a variation in the position/orientation of a functional group, linker or solvent molecule), or temporal (resulting from the dynamics of linkers, adsorbed solvent or guest molecules), structure solution using XRD is further complicated. As many of the interesting properties of solids arise from deviations in long-range periodicity, spectroscopic techniques that probe the local, atomic-scale structure can often be a useful and complementary approach for characterising ZIFs.

NMR spectroscopy has been widely used to investigate the structure of many solids, owing to its sensitivity to the local environment, without the need for any long-range order [15–17]. This is a suitable approach for studying ZIFs, owing to the variety of NMR-active nuclides present [17,18]. ^{1}H, ^{13}C and ^{15}N NMR spectroscopy can, in principle, be used to investigate the number, type and relative proportions of the framework linkers. The strong dipolar couplings present for ^{1}H result in a significant spectral broadening that limits resolution (and the extraction of structural information) unless very fast magic-angle spinning (MAS) is used [15,16]. For both ^{13}C and ^{15}N, the low sensitivity (resulting primarily from their low natural abundances of 1% and 0.34%, respectively) can be overcome by cross polarisation (CP) [15,16], where magnetisation is transferred from spatially close spins with high γ and high abundance (typically ^{1}H). While resulting in a considerable sensitivity enhancement (the maximum depending upon γ_H/γ_X), this approach does have the disadvantage of being non quantitative (as the transfer depends on the spatial proximity of the two species), and direct integration of the spectral resonances does not necessarily result in accurate relative proportions of chemical species unless they have a similar environment. In principle, spectroscopic study of the metal centres in ZIFs would provide information on the coordination environment and the framework topology [17,18]. However, many typical framework metals have relatively unfavourable NMR properties. For example, Zn (used in this work) has only one NMR-active isotope (^{67}Zn, I = 5/2) with a relatively low γ and low natural abundance of 4.1% (resulting in a receptivity, relative to ^{1}H, of 1.18×10^{-4}). Spectral acquisition is further hindered by the presence of a relatively large quadrupole moment (which, coupled with the low γ, produces significant quadrupolar broadening), often necessitating the use of high magnetic fields [19–22].

Even when resolution is increased through the use of techniques such as MAS, complex and overlapping spectral lineshapes are often still observed in NMR spectra of solids, particularly for disordered materials [23]. In recent years, there has been increasing interest in the use of computation (typically using density functional theory or DFT) to predict NMR parameters for periodic solids, aiding the interpretation and

assignment of spectra [24,25]. While extremely valuable in many cases, this can prove challenging if there are a large number of distinct atoms in the unit cell (as is the case for many ZIFs) or if there is significant disorder and/or dynamics of the linkers, functional groups or incorporated solvent/guest molecules. In these cases, it can be difficult to obtain a structural model that is a good approximation to the material studied experimentally, unless a very large number of possibilities are considered. One option is the use of cluster calculations, centred on the metal ion and incorporating the set of coordinating linkers, thereby circumventing problems with large cell sizes or disordered solvents. However, interactions between the framework and incorporated guests/solvents are not captured in this approach. Alternatively, periodic calculations (considering an unperturbed extended framework) can be employed, with solvent molecules either placed manually or removed entirely. The latter strategy may, however, lead to significant changes in the pore structure under geometry optimisation processes designed to minimise the forces upon atoms to ensure low-energy structures are considered, and may be less relevant to the actual material under study.

Owing to the difficulties in exploiting computational approaches for ZIFs, the amount and accuracy of the information that can be obtained from experimental measurements becomes increasingly important. There are many well-known empirically-derived relationships that link the isotropic chemical shift with the type of structural environment, and even to specific geometrical parameters, such as bond distances and angles [15,16]. However, additional information can be obtained by measuring the chemical shift anisotropy (CSA), thereby increasing confidence in the spectral assignments. Although this interaction is removed under the rapid MAS that is usually employed to achieve high-resolution experiments, the anisotropic shielding parameters can, in principle, be obtained from analytical fitting of the spinning sideband manifold observed in slow MAS experiments [15,16]. However, for systems with multiple distinct species the overlap of sideband and centreband signals can lead to difficulties in extracting this information. A number of experiments have been developed to overcome this problem, with the anisotropic information reintroduced or "recoupled" in the indirect dimension of a two-dimensional experiment, producing a sideband manifold that can be analysed to yield the desired information [26,27]. For nuclear sites that possess high local symmetry, resulting in small anisotropies, "amplification" experiments have also recently been developed [27], increasing the apparent magnitude of the interaction (by a user-defined scaling factor) and enabling more accurate measurement. The experiment used in this work, the CSA-amplified PASS approach [28,29], has been used successfully to investigate ^{1}H, ^{13}C, ^{31}P and ^{89}Y local environments in a range of materials, and correlations with local structural parameters, *e.g.*, bond distances or point symmetry, demonstrated [29–33].

For ZIFs, solid-state NMR spectroscopy can provide information on the type and relative proportions of linkers present, and the number of crystallographically-distinct molecules present in the asymmetric unit. Furthermore, it may be possible to distinguish between ZIFs that contain the same linker(s) but exhibit different three-dimensional topologies, through small variations in the chemical shifts, peak splittings or changes to the CSA. A number of authors have acquired conventional solid-state NMR spectra (primarily ^{13}C CP MAS spectra) [1,18,34], of individual ZIFs, but little attention has been focussed on the information (if any) available from the CSA, and upon the extent to which NMR parameters vary as the topology or extended structure is changed. It is not clear whether it is possible to unambiguously establish the presence of a linker in an unknown material simply from the shifts observed in a MAS spectrum, or whether additional confirmation from CSA measurements or ^{15}N NMR is required, or if the longer-range structure has a more significant effect. A more detailed understanding of the sensitivity of a more complete set of NMR parameters (*i.e.*, ^{13}C and ^{13}N isotropic and anisotropic shifts) to local structure will aid future solution of unknown structures, and help to understand the changes in the local environment upon the addition of guest molecules. In this work, we fully assign both ^{13}C and ^{15}N MAS NMR spectra of a variety of (single and dual linker) ZIFs, accurately measure CSA parameters and attempt to understand the relationships between NMR parameters and both local and long-range structure.

2. Methodology

2.1. Synthesis and basic characterisation

All ZIFs were prepared according to the previously reported literature procedures with some minor modifications (see the Supporting Information) [1,3,11,35,36]. In a typical synthesis (here for ZIF-7 [35]), benzimidazole (0.41 g, 3.47 mmol), zinc acetate dihydrate (0.56 g, 2.55 mmol), diethylamine (4.4 mL) and N,N-dimethylformamide (25 mL) were stirred (room temperature, 10 min). The mixture was placed into a Teflon™-lined steel autoclave and heated in an oven (110 °C, 2 days). The ZIF-7 product was collected by centrifugation and the wet solid was left in air, overnight. To further dry the product it was immersed in methanol (10 mL, room temperature, 9 h) and the resulting solid was collected by centrifugation. The white powder (typically 0.6 g, 24% yield with respect to benzimidazole) was then dried in an oven (90 °C, 15 h). Powder XRD data of the synthesised materials were collected in house using a Stoe STAD i/P diffractometer in capillary mode using Debye-Scherrer geometry with primary monochromation and Cu $K_{\alpha 1}$ (λ = 1.54051 Å) radiation. The collected patterns were then compared with simulated XRD patterns using crystal structures from the literature.

2.2. Solid-state NMR spectroscopy

Solid-state NMR spectra were acquired using Bruker Avance III spectrometers equipped with a 14.1 and 9.4 T widebore superconducting magnets operating at Larmor frequencies of 150.9 and 100.6 MHz for ^{13}C, and 60.8 and 40.6 MHz for ^{15}N, respectively. Samples were packed in conventional 4.0 mm rotors and rotated at MAS rates of 5 kHz (^{15}N) or 12.5 kHz (^{13}C). Chemical shifts are referenced to TMS using L-alanine as a secondary reference (δ(**C**H$_3$) = 20.5 ppm) for ^{13}C, and to nitromethane, using ^{15}N-enriched glycine as a secondary reference (δ(**N**H$_3$) = −347.4 ppm) for ^{15}N [16]. Spectra were acquired using CP, with a contact pulse (ramped for ^{1}H) between 1 and 5 ms (^{13}C), and 10 ms (^{15}N) duration. Continuous wave (cw), TPPM-15 [37] or SPINAL-64 [38] ^{1}H decoupling was employed to improve spectral resolution, with a typical radiofrequency field strength ($\gamma B_1/2\pi$) of ~100 kHz. Dipolar dephasing experiments were also carried out with similar parameters and a dephasing interval of 1 ms. Two-dimensional CP CSA-amplified PASS experiments were performed using the pulse sequence of Orr et al. [28,29] The total scaling factor is given by $N_T = (n_{PASS} + 1)N$, where N is the scaling factor determined by the timing of the five π pulses and n_{PASS} is the number of additional five π pulse blocks. Cogwheel phase cycling was employed to reduce the length of the phase cycle required [39]. See the Supporting Information for detailed parameters. Fitting of the sideband manifolds was performed using SIMPSON [40] by comparison to an ideal one-dimensional MAS spectrum. The "root mean square" (rms) error quoted in tables and plotted in figures is that output by SIMPSON, as described in the SIMPSON manual [40]. Using the Herzfeld-Berger convention [41], the isotropic chemical shift, δ_{iso}, is given by

$$\delta_{iso} = (\delta_{11} + \delta_{22} + \delta_{33})/3, \quad (1)$$

where, for the principal tensor components, $\delta_{11} \geq \delta_{22} \geq \delta_{33}$. The magnitude of the anisotropy is defined by the span

$$\Omega = \delta_{11} - \delta_{33}, \quad (2)$$

and the shape is defined by the skew

$$\kappa = 3\,(\delta_{22} - \delta_{iso})/\,\Omega, \quad (3)$$

such that κ lies between 1 and –1. Alternative conventions for describing the shielding interaction, in terms of the anisotropy and asymmetry, can be found in Ref. [42].

2.3. DFT calculations

Calculations of total energies and NMR parameters were carried out using the DFT code CASTEP [43] (version 16.1), which employs the gauge-including projector augmented wave (GIPAW [44]) approach, to reconstruct the all-electron wavefunction in the presence of a magnetic field. Calculations were carried out using the GGA PBE [45] functional and core-valence interactions were described by ultra-soft pseudopotentials [46]. A planewave cutoff energy of 50 Ry (~680 eV) was used, and integrals over the Brillouin zone were performed using a Monkhorst–Pack grid with a k-point spacing of 0.04 2π Å^{-1}. The TS semi-empirical dispersion correction scheme [47,48] was used. All calculations were converged as far as possible with respect to both k-point spacing and cutoff energy. Prior to the calculation of NMR parameters, structural models were obtained from the CCDC (see Table 1 for codes). Atoms related to the solvent molecules were removed and the geometry of the models optimised to an energy minimum (with all atomic coordinates and the size/shape of the unit cell allowed to vary) using the same parameters stated above. Calculations were performed either on a cluster at the University of St Andrews, consisting of 300 12-core Intel Westmere nodes, connected with QDR Infiniband, or on ARCHER, the UK High Performance Computing service, consisting of a Cray XC30 MPP supercomputer with 4920 24-core Intel Ivy Bridge nodes. Calculation wallclock times ranged from 4 to 8 days using 16–32 nodes. For further details (including information on initial models and geometry optimisation) see the Supporting Information.

Calculations generate the absolute shielding tensor ($\boldsymbol{\sigma}$) in the crystal frame, and diagonalisation of the symmetric part of $\boldsymbol{\sigma}$ yields the three principal components, σ_{11}, σ_{22} and σ_{33}. The principal components of the chemical shift tensor, δ_{11}, δ_{22} and δ_{33} are related to $\boldsymbol{\sigma}$ by

$$\delta_{ii} = -(\sigma_{ii} - \sigma_{ref})/(1 - \sigma_{ref}) \approx -(\sigma_{ii} - \sigma_{ref}), \quad (4)$$

where σ_{ref} (assumed to be << 1) is the reference shielding. Values of σ_{ref} of 175.47 ppm and −136.26 ppm were used for ^{13}C and ^{15}N, respectively, determined from a comparison of the experimental shifts and calculated shieldings of all ZIFs studied in this work.

3. Results and discussion

Fig. 2 shows ^{13}C CP MAS NMR spectra of Zn-containing ZIF-7, ZIF-8, ZIF-11, ZIF-20, ZIF-65, ZIF-68, ZIF-70 and ZIF-78 (see Fig. 1 and Table 1 for information on the linkers used and topologies formed in each case). The presence of disordered or dynamic solvent molecules, and of multiple, but chemically similar, linkers can complicate the assignment of NMR spectra of ZIFs. In many of the spectra in Fig. 2, peaks associated with the synthesis solvent, DMF, can be seen (indicated by †) at chemical shifts of ~30, ~35 and ~160 ppm. In ZIF-11, peaks from the toluene solvent are seen (indicated by ‡) at 129.7 and 128.3 ppm. In addition, spinning sidebands are seen in all spectra (indicated by *), suggesting that many sites do exhibit a significant CSA, as would be expected for sp^2 C. With the exception of ZIF-8 (where a peak at 14.9 ppm is observed for the CH_3 group on the mIm linker) all resonances associated with the linker are found between 100 and 160 ppm, indicating the aromatic nature of the linkers and the presence of the diamagnetic Zn metal centre.

For ZIFs with single linkers (ZIF-7, ZIF-8, ZIF-11, ZIF-20 and ZIF-65) the chemical shifts observed are similar to those found in solution-state NMR spectra of the linker molecules, enabling tentative spectral assignment, and also suggesting that the longer-range structure (*i.e.*, the exact framework topology) has a limited effect on the chemical shifts observed in the solid state. Assignments were supported by dipolar dephasing experiments, where the reintroduction of the ^{1}H/^{13}C dipolar coupling

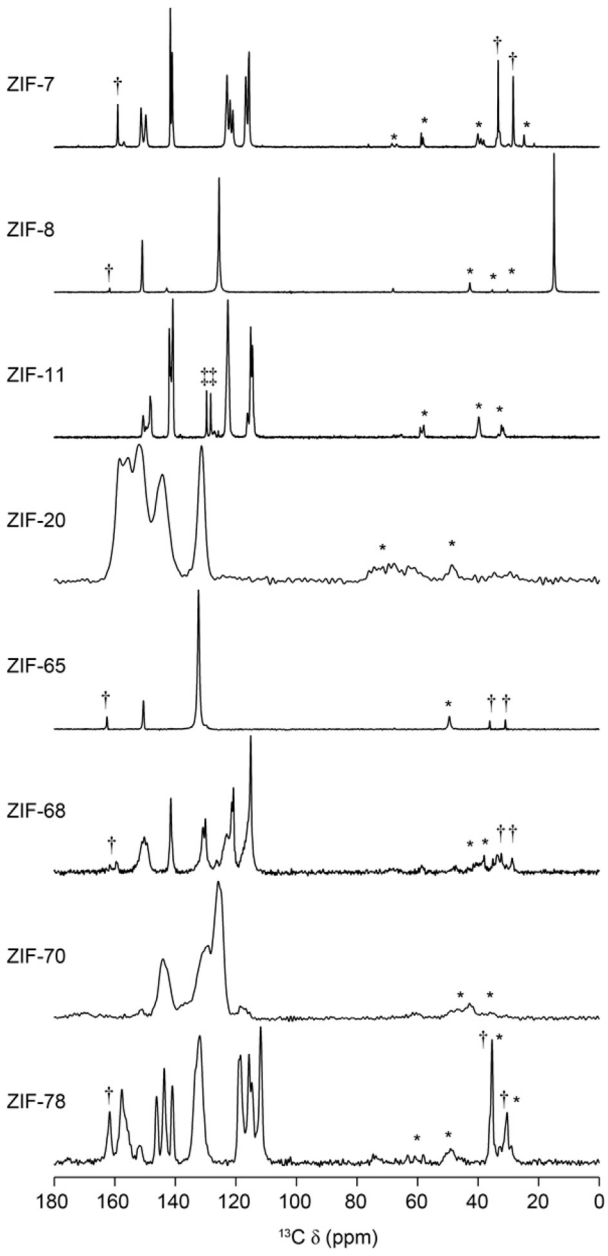

Fig. 2. ^{13}C (14.1 T, 12.5 kHz) CP MAS NMR spectra of single- and dual-linker ZIFs. Peaks associated with the synthesis solvents are indicated by † (DMF) and ‡ (toluene). Spinning sidebands are indicated by *.

enables quaternary and protonated C species to be distinguished. For all ZIFs, spectra with dephasing times of 1 ms are shown in the Supporting Information, along with a more detailed discussion of the spectral assignment. For ZIF-20, assignment of the ^{13}C spectrum is challenging, owing to the broader, overlapped spectral lineshapes, and the chemical similarity of many of the C species present. Partial assignment can be made from the dipolar dephasing spectra, but an unambiguous assignment is not possible. A summary of the proposed assignments for all ZIFs is given in Table 2. In many cases, the spectral broadening (present as a result of disordered linkers or solvent molecules) makes it difficult to determine unambiguously the number of crystallographically-distinct linkers that are present in the materials, although for ZIF-8 and ZIF-65 it is clear only one set of resonances are seen. For ZIF-7, the sharp lines suggest a relatively ordered structure, and two distinct resonances are clearly seen for most C species, consistent with the presence of two crystallographically-distinct linkers [35]. Some additional splitting is

Table 2
Experimental ^{13}C (14.1 T) NMR parameters (δ_{iso}, Ω, κ) and rms errors, along with the assignment of resonances observed for a range of single-linker ZIFs.

	δ_{iso} (ppm)	Ω (ppm)	κ	rms error	Assignment	
ZIF-7	151.3 ± 0.1	134.7 ± 7.1	0.0 ± 0.1	1.38	N—***C***(H)—N	C2
	149.7 ± 0.1	134.6 ± 7.3	−0.1 ± 0.1	4.07	N—***C***(H)—N	C2
	141.6 ± 0.1	148.9 ± 6.8	−0.5 ± 0.1	0.57	N—***C***=***C***—N	C3
	141.1 ± 0.1	149.0 ± 6.3	−0.5 ± 0.1	1.53	N—***C***=***C***—N	C3
	122.9 ± 0.1	185.8 ± 9.8	−0.2 ± 0.1	1.38	N—C—***C***H=CH	C4
	121.9 ± 0.1	185.6 ± 10.1	−0.1 ± 0.1	2.30	N—C—***C***H=CH	C4
	121.0 ± 0.1	189.0 ± 9.4	−0.2 ± 0.1	1.32	N—C—***C***H=CH	C4
	116.7 ± 0.1	162.4 ± 7.7	−0.3 ± 0.1	0.99	N—C—CH=***C***H	C5
	115.7 ± 0.1	158.4 ± 7.8	−0.3 ± 0.1	0.57	N—C—CH=***C***H	C5
ZIF-8	150.9 ± 0.1	139.2 ± 6.7	−0.1 ± 0.1	0.80	N—***C***(CH_3)—N	C2
	125.6 ± 0.1	139.0 ± 7.0	0.2 ± 0.1	0.58	N—***C***H=***C***H—N	C3
	14.9 ± 0.1				—***C***H_3[a]	C4
ZIF-11	150.5 ± 0.1	122.2 ± 7.7	0.0 ± 0.1	6.02	N—***C***(H)—N	C2
	148.3 ± 0.1	122.5 ± 7.9	0.0 ± 0.1	4.32	N—***C***(H)—N	C2
	141.9 ± 0.1	145.7 ± 6.0	−0.5 ± 0.1	0.52	N—***C***=***C***—N	C3
	141.5 ± 0.1	144.4 ± 6.1	−0.6 ± 0.1	0.26	N—***C***=***C***—N	C3
	140.8 ± 0.1	140.9 ± 5.9	−0.5 ± 0.1	0.22	N—***C***=***C***—N	C3
	122.6 ± 0.1	173.8 ± 10.3	−0.1 ± 0.1	0.81	N—C—***C***H=CH	C4
	116.1 ± 0.1	160.2 ± 9.2	−0.3 ± 0.1	17.14	N—C—CH=***C***H	C5
	115.0 ± 0.1	162.3 ± 8.6	−0.2 ± 0.1	0.89	N—C—CH=***C***H	C5
	114.4 ± 0.1	158.1 ± 7.9	−0.2 ± 0.1	0.20	N—C—CH=***C***H	C5
ZIF-20	158.4 ± 0.5	159.7 ± 7.7	−0.4 ± 0.1	8.88	N—***C***(=C—N)—N	C9/4
	155.7 ± 0.5	163.3 ± 7.3	−0.4 ± 0.1	1.37	N—***C***(H)—N	C2/5/7
	152.0 ± 0.5	150.9 ± 8.4	−0.2 ± 0.1	7.20	C—***C***H=N—CH	C2/5/7
	144.5 ± 0.5	155.9 ± 7.3	−0.5 ± 0.1	7.25	N=***C***H—N	C2/5/7
	131.4 ± 0.5	141.8 ± 7.1	−0.2 ± 0.1	6.71	N—***C***=C—N	C9/4
ZIF-65	150.6 ± 0.1	82.1 ± 5.1	0.4 ± 0.1	0.52	N—***C***(NO_2)—N	C2
	132.6 ± 0.1	133.8 ± 8.0	0.0 ± 0.1	2.53	N—***C***H=***C***H—N	C3

[a] Insufficient number of data points to determine the CSA parameters accurately.

observed at lower shifts (δ between 120 and 124 ppm), suggesting some additional disorder, most likely as a result of the incorporated solvent. ZIF-7 and ZIF-11 contain the same bIm linker, but the different synthetic routes produce ZIFs with different zeolite topologies (SOD and RHO, respectively). Although the chemical shifts observed are very similar, the exact resonance positions are different. This suggests that although the chemical shift primarily indicates the chemical nature of the linker, the ^{13}C NMR spectra will be sensitive to changes in the structure, *i.e.*, upon loading of guest molecules or changes in symmetry. As an example, ^{13}C NMR spectroscopy was used to distinguish the three crystallographically-distinct types of nIm linker in $Zn(nIm)_2$, and to confirm the presence of rotational disorder for one of the three [49]. Furthermore, ^{13}C spectra could distinguish between the different polymorphic forms of this material, showing changes upon an increase in temperature [49]. Additional information on a larger number of ZIFs that contain the same linker but exhibit different topologies (and/or *vice versa)* is required to investigate the structure sensitivity of NMR further.

In addition to the isotropic chemical shift, solid-state NMR also enables access to the anisotropic component (parameterised by Ω and κ) of this interaction. Although these are typically removed under the sample rotation used to achieve high resolution, they can be measured either from a slow MAS spectrum or from the sideband pattern in the indirect dimension of a two-dimensional experiment that recouples, or selectively reintroduces, the anisotropic shielding [26,27]. It has been shown that the anisotropic shielding, the asymmetry and the tensor orientation can provide information on the local structure including, *e.g.*, bond distances and point symmetry [15,16,24,30]. Given the complexity of the ^{13}C spectra of most ZIFs, slow MAS experiments result in considerable spectral overlap, and CSA-amplified PASS experiments have been used to reintroduce and measure the anisotropic shielding. Fig. 3a shows an example of a ^{13}C two-dimensional CSA-amplified PASS spectrum (for ZIF-65), along with the extracted sideband manifolds for the two C sites in the nIm linker. A scaling factor, N_T, of 5 was used, resulting in an apparent MAS rate in the indirect dimension of 2.5 kHz. Fig. 3b shows the contour plots of the rms deviation found for analytical fitting of each sideband manifold (arbitrarily limited to 25). Values of Ω and κ extracted from similar spectra for all single-linker ZIFs are given in Table 2. The low rms deviations observed for ZIF-7, ZIF-8 and ZIF-11 indicate that accurate values can be extracted, although for ZIF-8 it is not possible to measure

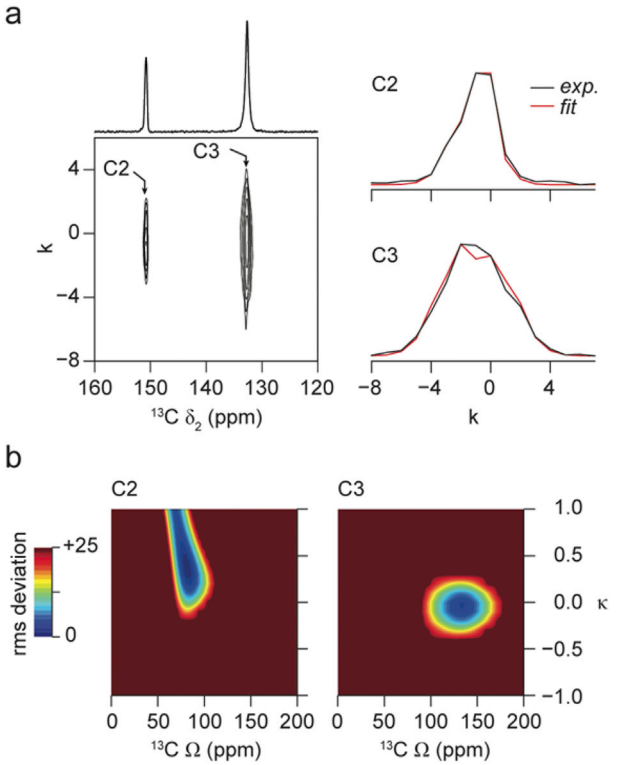

Fig. 3. (a) ^{13}C (14.1 T, 12.5 kHz) two-dimensional amplified-PASS spectrum (N_T = 5) of ZIF-65, with extracted sideband manifolds and corresponding fits for the two distinct C sites. The spinning sideband order is denoted k. (b) Two-dimensional contour plots showing the rms error of the analytical fitting of each sideband manifold for values of the span, Ω, and the skew, κ. The intensity scale of the plots has been (arbitrarily) limited to 25.

the CSA parameters for C4 of the mIm linker ($\delta_{iso} = 14.9$ ppm), owing to the very small magnitude of this interaction (and the insufficient number of sidebands produced even when the CSA is amplified). For ZIF-20, the higher rms error suggests greater uncertainties in the values determined, probably as a result of the greater overlap of the spectral resonances arising from the similarity in the C environments of the pur linker. The proposed crystal structure for ZIF-20 does suggest some disorder in the exact orientation of the linker molecules, with the positions of C and N in the six-membered ring not defined [35].

Table 2 shows that in many cases the range of Ω for a type of C species is greater than that of the corresponding δ_{iso} values, potentially enabling better distinction between ZIFs with similar linkers but different topologies, and a greater sensitivity to small structural changes upon loading or post-synthetic modification. For example, for the C2 (N—***C***(X)—N) sites in ZIF-7 (X = H), ZIF-8 (X = CH_3), ZIF-11 (X = H) and ZIF-65 (X = NO_2) δ_{iso} lies between 148 and 151 ppm (despite the different chemical nature of these species), but Ω varies from 82 to 139 ppm. Although it can be difficult to relate the anisotropic shielding parameters directly to the symmetry and arrangement of the coordinating atoms in anything other than the simplest molecular systems, it is noticeable that a much lower Ω (82 ppm) is observed for ZIF-65, perhaps reflecting more symmetrical arrangement of the atoms bonded to C2 in this linker (*i.e.*, three N atoms, rather than two N and one C). There is also a more significant change in κ for this species. Furthermore, for the two ZIFs with bIm linkers (ZIF-7 and ZIF-11) δ_{iso} for the N—C—***C***H═CH species (C4) is very similar (*i.e.*, within 1 ppm), while there is a ~15 ppm difference in Ω.

In ZIFs the N atoms on the imidazolate ring coordinate to the metal centre (in this case Zn^{2+}). In principle, N NMR could provide information on the linker(s) present, but may also be more sensitive to the Zn coordination environment (and also, therefore, to the framework topology). Furthermore, as there are typically fewer crystallographically-unique nitrogen species in ZIFs, it should be more straightforward to assign N NMR spectra than the corresponding ^{13}C NMR spectra. There are two NMR-active isotopes of N, ^{14}N and ^{15}N. Although ^{14}N has the much higher natural abundance (~99.7%), it also has spin quantum number I = 1, resulting in lineshapes that are broadened by the quadrupolar interaction. However, although having I = 1/2, the low natural abundance and low γ of ^{15}N, results in very poor sensitivity (receptivity relative to ^{1}H is 1.04×10^{-3}), resulting in long experimental times unless efficient CP can be achieved [15,16]. Fig. 4 shows ^{15}N CP MAS NMR spectra of the single-linker ZIFs, ZIF-7, ZIF-8, ZIF-11, ZIF-20 and ZIF-65. (Peaks due to the spinning sidebands are indicated by *). Sharp ^{15}N spectral resonances can be observed for ZIF-7, ZIF-8 and ZIF-65, reflecting the ordered nature of these materials. For ZIF-20, broader spectral lines are observed, resulting from the disorder in the material discussed previously. Proposed assignments of the ^{15}N spectra are given in Table 3.

For ZIF-7, two ^{15}N resonances are observed in a 3:1 ratio, attributed to the four chemically-similar but crystallographically-distinct nitrogen sites in the proposed crystal structure, suggesting that three of the nitrogen species have very similar (although not identical) NMR parameters. The same bIm linker is present in ZIF-11 and, while similar chemical shifts are observed, the ^{15}N CP MAS spectrum is different in detail from that of ZIF-7, with ~4 distinct N shifts present (although each has a different intensity). Although there are four formally crystallographically-distinct N species predicted in the crystal structure (as with ZIF-7), there is also some uncertainty over the exact orientation of the bIm linker [1], leading to the additional splittings and line broadening observed in the spectrum. The ^{15}N chemical shifts for the ZIFs containing mIm and nIm differ from those with bIm (with downfield shifts of between 15 and 20 ppm observed for the linker N). For ZIF-65, a second N resonance is seen at −27 ppm, corresponding to —***N***O_2 (N4). The two broad resonances for the pur linker (at −121 and −192 ppm) can be assigned as N6/N8 and N1/N3, respectively, by comparison to the other ZIFs. Although, in general, the chemical shifts observed reflect the chemical nature of the linker, the ^{15}N CP MAS spectra do appear to be more sensitive to changes in topology or variation in the local geometry around the metal centre than the corresponding ^{13}C spectra, enabling different ZIFs to be more easily distinguished.

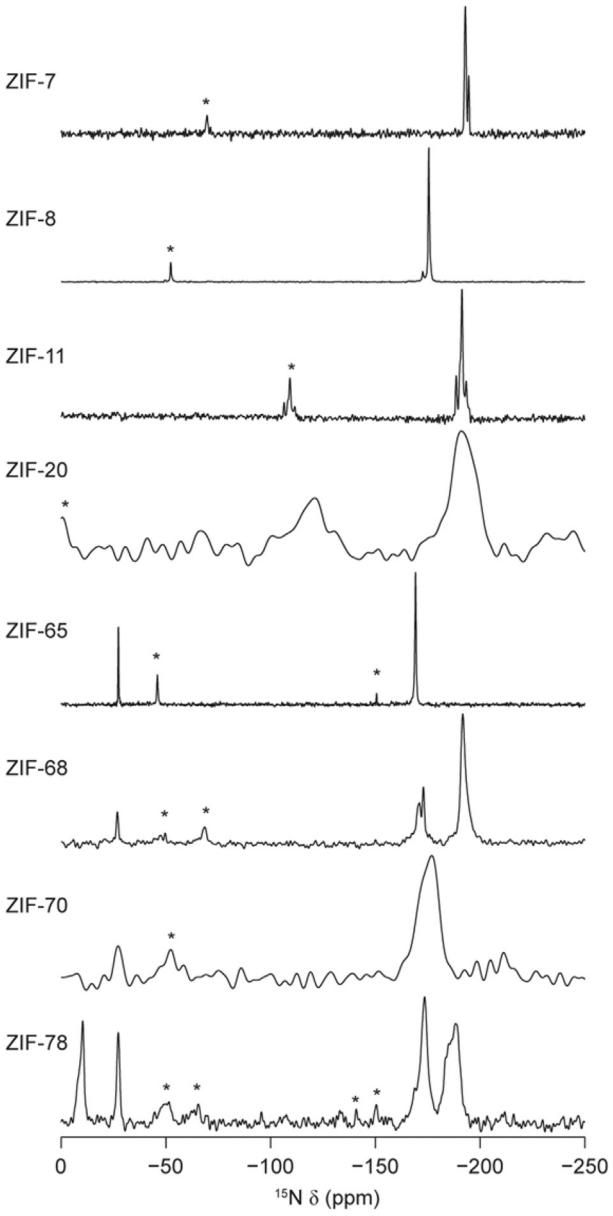

Fig. 4. ^{15}N (14.1 T, 5 kHz) CP MAS NMR spectra of single- and dual-linker ZIFs. Spinning sidebands are indicated by *.

^{15}N CSA-amplified PASS experiments were also performed for the single-linker ZIFs, and the values of Ω and κ extracted are given in Table 3. Owing to the broad resonances observed for ZIF-20, it was not possible to obtain the CSA parameters for this material on a reasonable timescale. In general, Ω for the imidazolate N species varies between 167 and 308 ppm, with the largest value (for the ***N***—C(NO_2)—***N*** environment) seen for ZIF-65. The relatively low rms values (Table 3) reveal the good confidence in the fits, suggesting that the ^{15}N Ω is less dependent purely on the chemical nature of the linker (and more sensitive to the three-dimensional structure). For example, for the four imidazolate N species in ZIF-11 (all chemically equivalent) a spread of nearly 50 ppm in Ω is observed. Although Ω for the —***N***O_2 group in the nIm linker in ZIF-65 is one of the largest measured, and larger than most Ω values for the heterocyclic N species, it is similar to the imidazolate N for this ZIF.

Table 3
Experimental ^{15}N (9.4 T) NMR parameters (δ_{iso}, Ω, κ) and rms errors, along with the assignment of resonances observed for a range of single-linker ZIFs.

	δ_{iso} (ppm)	Ω (ppm)	κ	rms error	Assignment	
ZIF-7	−192.6 ± 0.1	233.5 ± 17.2	0.7 ± 0.2	3.03	***N***—C(H)—***N***	N1
	−194.2 ± 0.1	250.9 ± 12.0	0.3 ± 0.2	2.75	***N***—C(H)—***N***	N1
ZIF-8	−175.5 ± 0.1	241.0 ± 12.2	0.9 ± 0.1	0.51	***N***—C(CH_3)—***N***	N1
ZIF-11	−188.6 ± 0.1	215.4 ± 12.3	0.5 ± 0.2	3.96	***N***—C(H)—***N***	N1
	−190.3 ± 0.1	175.1 ± 16.2	0.8 ± 0.1	5.81	***N***—C(H)—***N***	N1
	−191.3 ± 0.1	172.0 ± 11.8	1.0 ± 0.1	1.35	***N***—C(H)—***N***	N1
	−193.4 ± 0.1	167.1 ± 12.1	0.8 ± 0.1	1.93	***N***—C(H)—***N***	N1
ZIF-20[a]	−192.1 ± 0.5					N1+N3
	−120.8 ± 0.5					N6+N8
ZIF-65	−27.2 ± 0.1	290.9 ± 15.4	0.3 ± 0.1	0.54	C(***N***O_2)	N4
	−169.2 ± 0.1	308.6 ± 15.8	0.6 ± 0.1	0.51	***N***—C(NO_2)—***N***	N1

[a] Signal intensity too low to extract CSA parameters accurately.

As described above, it is difficult to perform first-principles calculations to aid in spectral assignment or to provide support for the experimental values measured, owing to the large size of many ZIF systems and the disorder/dynamics of the solvent molecules present (many of which are not placed accurately in models derived from diffraction). It is, however, possible to calculate NMR parameters for ZIFs where all solvent/water molecules have been removed from the pores. While this is not necessarily a true reflection of the as-prepared materials under experimental study here, it can potentially provide a better representation of the chemical nature of the system (*i.e.*, Im linkers attached to Zn^{2+} cations in a three-dimensional extended structure) and, therefore, more accurate NMR parameters can be obtained, than solution-state NMR spectra of the neutral linker molecules. Periodic DFT calculations were carried out for ZIF-7, ZIF-8 and ZIF-65 (*i.e.*, single-linker ZIFs with no framework disorder). Any atoms from solvent molecules present in the diffraction-based structural models were removed from the pores (see the Supporting Information for further discussion). Table 4 shows the calculated ^{13}C and ^{15}N NMR parameters for these three ZIFs. Although the exact values of δ_{iso} and Ω do not match experiment exactly, as perhaps expected owing to the changes made to the structure, they are in good qualitative agreement and can be used to confirm the spectral assignments given in Tables 2 and 3 This can be seen clearly in the plots of calculated against experimental NMR parameters shown in the Supporting Information. In particular, for ZIF-7 (and, by analogy, ZIF-11) they suggest that δ_{iso} values for C4 and C5 (on the benzene ring of the bIm linker) are 121–123 and 116–117 ppm, respectively, (rather than *vice versa*), in contrast to the assignment that would be indicated if solution-state NMR shifts only were used. It is noticeable for ZIF-8 that the agreement between experiment and calculation for Ω is poorer than for the other ZIFs, perhaps reflecting the dynamics of the —CH_3 group.

Table 4
Calculated (using CASTEP), ^{13}C and ^{15}N NMR parameters (δ_{iso}, Ω, κ) for ZIF-7, ZIF-8 and ZIF-65.

		δ_{iso} (ppm)	Ω (ppm)	κ	Assignment	
ZIF-7	^{13}C	153.35	149.10	−0.08	N—***C***(H)—N	C2
		151.58	148.63	−0.01	N—***C***(H)—N	C2
		147.84	166.14	−0.57	N—***C***═***C***—N	C3
		147.76	166.84	−0.57	N—***C***═***C***—N	C3
		147.69	169.17	−0.61	N—***C***═***C***—N	C3
		147.53	169.77	−0.61	N—***C***═***C***—N	C3
		129.33	224.11	−0.18	N—C—***C***H═CH	C4
		128.91	223.69	−0.15	N—C—***C***H═CH	C4
		127.59	223.01	−0.15	N—C—***C***H═CH	C4
		127.23	223.69	−0.15	N—C—***C***H═CH	C4
		121.90	198.40	−0.29	N—C—CH═***C***H	C5
		121.89	197.89	−0.29	N—C—CH═***C***H	C5
		120.73	193.27	−0.30	N—C—CH═***C***H	C5
		120.72	192.14	−0.28	N—C—CH═***C***H	C5
	^{15}N	−195.02	255.02	−0.66	***N***—C(H)—***N***	N1
		−193.36	258.80	−0.69	***N***—C(H)—***N***	N1
		−194.77	253.63	−0.67	***N***—C(H)—***N***	N1
		−192.38	261.04	−0.69	***N***—C(H)—***N***	N1
ZIF-8	^{13}C	155.01	135.22	−0.23	N—***C***(CH_3)—N	C2
		130.94	155.55	0.15	N—***C***H═***C***H—N	C3
		129.56	152.58	0.14	N—***C***H═***C***H—N	C3
		14.90	22.75	−0.91	N—C(***C***H_3)—N	C4
	^{15}N	−175.50	281.88	−0.69	***N***—C(CH_3)—***N***	N1
		−173.81	271.67	−0.74	***N***—C(CH_3)—***N***	N1
ZIF-65	^{13}C	157.5	78.90	−0.03	N—***C***(NO_2)—N	C2
		139.40	157.95	−0.08	N—***C***H═***C***H—N	C3
		139.40	157.95	−0.08	N—***C***H═***C***H—N	C3
	^{15}N	−170.71	322.32	−0.64	***N***—C(NO_2)—***N***	N1
		−170.71	322.32	−0.64	***N***—C(NO_2)—***N***	N1
		−46.88	272.58	−0.10	C(***N***O_2)	N4

More complex ZIFs can be synthesised using more than one type of linker, producing materials that not only have different pore shapes and sizes, but that can also have different chemical properties (*e.g.*, hydrophobic or hydrophilic pores) [2,4–9]. The ^{13}C CP MAS NMR spectra of ZIF-68, ZIF-70 and ZIF-78 are shown in Fig. 2, with expansions also shown in Fig. 5. These dual-linker ZIFs all possess the same topology (GME) [3,11], and all contain the nIm linker. However, the second linker for each ZIF varies, as shown in Table 1, with bIm for ZIF-68, Im for ZIF-70 and nbIm for ZIF-78. The increased complexity of the spectra (particularly in the crowded aromatic region) make assignment more challenging, and DFT calculations are not feasible (owing to the size of the unit cell and potential disorder of the linkers). Some progress can be made by comparing spectra to those for the single-linker ZIFs (Fig. 5 and Section S3 in the Supporting Information), and by using dipolar dephasing experiments (also in the Supporting Information). Furthermore, ^{13}C 2D CSA-amplified PASS experiments enable measurement of the anisotropic shielding parameters, and provide further support for the spectral assignment. The proposed assignments of the resonances are given in Table 5.

For ZIF-68, the spectrum contains resonances in very similar positions to those in ZIF-7/ZIF-11 (bIm linkers) and to those in ZIF-65 (nIm linker), enabling the type of C species to be easily assigned, as shown in Fig. 5. Likewise, for ZIF-70 and ZIF-78 peaks are also observed in very similar positions to those for the nIm linker in ZIF-65. For ZIF-70 very broad spectral lines are seen, reflecting the considerable disorder of the positions of the Im and nIm linkers in the structure. Although the resonances for ZIF-78 appear much narrower, many different resonances are present, reflecting the loss of the symmetry in the bIm linker through the introduction of the NO_2 group at the 6 position (see Fig. 1). Furthermore, the crystal structure suggests some uncertainty over the exact orientation of a portion of the nIm linkers, and also in the position of the NO_2 group on the nbIm ring, although the linkers do appear to be ordered in terms of their position within the structure. Although it is possible to assign a number of C species for this material, it is not possible to distinguish easily between the three quaternary C species in nbIm (C4, C6 and C9) or between the three nbIm aromatic CH species (C5, C7 and C8), as shown in Table 2 (although the quaternary and CH carbons are readily distinguished from each other by dipolar dephasing experiments – see Supporting Information). In general, it is clear that the observation made earlier, that ^{13}C δ_{iso} values depend primarily on the chemical nature of

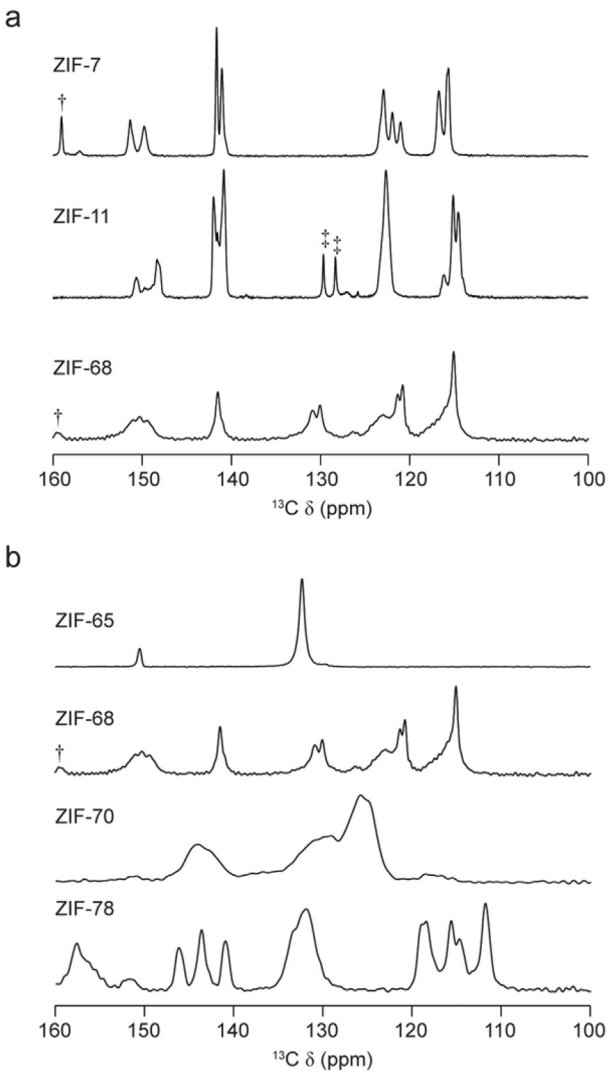

Fig. 5. Expansion of ^{13}C (14.1 T, 12.5 kHz) CP MAS NMR spectra of ZIFs containing (a) a bIm and (b) a nIm linker. Peaks associated with the synthesis solvents are indicated by † (DMF) and ‡ (toluene).

the linker and only to a lesser extent on longer-range structure and topology, proves to be extremely useful. When complex multi-linker ZIF structures are produced (and complex NMR spectra result), the linkers present can be identified (and spectra partially or wholly assigned) by comparison to simpler materials. In general, ^{13}C Ω also appears to be broadly similar to the values observed for single-linker ZIFs, but displays a greater variation than δ_{iso}. For example, C2 of the nIm linker varies between ~124 and 104 ppm (in ZIF-68), ~71 ppm (in ZIF-70), ~85 ppm (in ZIF-78), compared to ~82 ppm in the single-linker ZIF-65.

As with the single-linker ZIFs, the ^{15}N CP MAS spectra (shown in Fig. 4, with expansions given in the Supporting Information) of the dual-linker materials contain fewer resonances than the corresponding ^{13}C spectra. The values of ^{15}N δ_{iso} and of Ω and κ were extracted from CSA-amplified PASS experiments (where sufficient sensitivity was obtained) and are given in Table 6. The nIm —$\boldsymbol{N}O_2$ groups are straightforward to assign (by comparison to ZIF-65), with resonances in very similar positions in all three ZIFs (−26.9, −27.5, −27.1 ppm). For ZIF-78, the —$\boldsymbol{N}O_2$ group on the nbIm linker also appears with a very high chemical shift (−10.0 ppm). For all three dual-linker ZIFs, the nIm N species have very similar shifts to those found in ZIF-65, and the bIm N species in ZIF-68 can be assigned by comparison to ZIF-7. This leaves the peaks at *ca.* −185 ppm in ZIF-78 as the nbIm aromatic N species. For ZIF-70, it would appear that the Im N species overlap with those from nIm, producing a very broad resonance at *ca.* −176 ppm.

Although the exact ratio of the two (or, in some cases, more) linkers that are used in an initial synthesis is known exactly, these may not be incorporated into the final product in the same ratios. A related problem is encountered for aluminophosphate frameworks, where multiple structure-directing agents can be used in the synthesis, but are incorporated to a lesser extent (or in some cases not at all) into the final product [50]. Determining the relative proportion of linkers present is important for understanding the structure and chemical properties of a material (and for reproducing it accurately), but can pose a challenge for diffraction when very similar linkers (*e.g.*, those that differ only one functional group) are used, or where there is considerable disorder in the position of the linkers within the material. For example, in the original work, ZIF-70 was prepared using a 1:1 ratio of Im and nIm, but the final product exhibits a ratio of 1.3:1 (as determined from elemental analysis) [3]. One approach to investigate linker ratios is to use acid hydrolysis to decompose the framework into individual molecules and employ solution-state NMR spectroscopy. Clearly, this has the significant disadvantage of being a destructive technique that will be incompatible with some functional groups. In principle, the non-destructive approach of solid-state NMR spectroscopy should be ideally suited to investigate the proportions of linker present in the final material directly. However, as discussed above, CP is inherently non quantitative and, particularly for materials with many closely spaced or overlapped spectral lines, this can be a problem [15,16]. Although some advances towards quantitative CP measurements have been made recently using a multiple-contact method [51], this does rely and strongly-coupled ^{1}H spin baths and so has been suggested not to be of use in the more sparse ^{1}H distributions found in MOFs. Therefore, we have focussed only on the comparison of resonances from chemically-similar species in conventional CP spectra to investigate the linker ratios.

For ZIF-68, it is difficult to determine the linker ratio unambiguously, as the ^{13}C spectrum contains both sharp and broader resonances, and it is not clear if there is additional unreacted linker present within the pores. When considering the sharper peaks only, an integral ratio of ~1:1 would be obtained for the C3 (nIm) and C4 or C5 (bIm), suggesting that the linker ratio is also close to 1:1. The relative intensities of the imidazole N in the ^{15}N spectra are closer to 1:2 (nIm:bIm), but it should be noted that the N species differ in the number (and types) of surrounding H. As described in the Supporting Information, the nIm:bIm linker ratio determined from ^{1}H solution-state NMR of the digested ZIF was 1:2, in better agreement with the ^{15}N data. However, this value would be affected by the presence of any unreacted linker within the pores, as indicated by the ^{13}C solid-state NMR spectra. ZIF-70 also poses a challenge owing to the broad peaks resulting from the linker disorder. However, decomposition of the C3 peaks in the ^{13}C NMR spectrum, gives an approximate ratio of 1.5:1 for Im:nIm. It is not possible to resolve the two chemically-similar N1 species in the ^{15}N NMR spectrum. A solution-state ^{1}H NMR spectrum after digestion gave an Im:nIm ratio of 1.9:1, higher than the 1.3:1 observed in the original preparation of ZIF-70 [3]. It is not possible to resolve the two chemically-similar N1 species in the ^{15}N NMR spectrum. For ZIF-78, although the ^{13}C spectra cannot be fully assigned, the relative intensities of the C3 (nIm) and C5+C7+C8 (nbIm) signals are ~1:1.5 (or 2:3), as expected for a 1:1 ratio of the linkers. In the ^{15}N NMR spectrum, the relative intensity ratio of N1 (nIm) and N1+N3 (nbIm) is ~1:1.2 and, although the exact chemical environment of the imidazole N is different, the relatively low number of proximate H in each case probably supports the conclusion from the ^{13}C NMR spectrum. As expected, the relative ratios of the signals from the —$\boldsymbol{N}O_2$ groups are not in agreement (~1.8:1 for N4:N10), reflecting the greater number of nearby ^{1}H in the nbIm linker. The solution-state ^{1}H NMR spectrum of the digested ZIF confirmed a 1:1.1 (nIm:nbIm), in very good agreement with the solid-state NMR data.

Fig. 6a shows a plot of the experimental ^{13}C δ_{iso} against Ω for each resonance in the single- and dual-linker ZIFs (with the exception of ZIF-20). Symbols denote the chemical type of species/linker and these are

Table 5
Experimental ^{13}C (14.1 T) NMR parameters (δ_{iso}, Ω, κ) and rms errors, along with the assignment of resonances observed for a range of dual-linker ZIFs.

	δ_{iso} (ppm)	Ω (ppm)	κ	rms error	Assignment	
ZIF-68	151.1 ± 0.1	123.2 ± 8.0	0.2 ± 0.1	16.4	nIm: N—***C***-(NO_2)N	C2
	150.3 ± 0.1	103.6 ± 6.8	0.0 ± 0.1	7.14	nIm: N—***C***-(NO_2)N	C2
	149.2 ± 0.1	115.0 ± 7.8	0.1 ± 0.1	26.32	bIm: N—***C***(H)—N	C2
	141.7 ± 0.1	147.1 ± 6.9	−0.6 ± 0.1	1.67	bIm: N—***C***═***C***—N	C3
	131.3 ± 0.1	119.3 ± 8.1	0.0 ± 0.1	6.83	nIm: N—***C***H—***C***H—N	C3
	130.3 ± 0.1	127.3 ± 8.2	0.1 ± 0.1	4.74	nIm: N—***C***H—***C***H—N	C3
	121.6 ± 0.1	186.6 ± 12.1	−0.1 ± 0.1	9.65	bIm: N—C—***C***H═CH	C4
	120.7 ± 0.1	175.7 ± 9.8	0.0 ± 0.1	5.79	bIm: N—C—***C***H═CH	C4
	115.3 ± 0.1	151.5 ± 7.6	−0.2 ± 0.1	1.11	bIm: N—C—CH═***C***H	C5
ZIF-70	151.4 ± 1.0	70.6 ± 4.9	0.4 ± 0.1	26.50	nIm: N—***C***(NO_2)—N	C2
	144.4 ± 1.0	119.1 ± 7.9	0.0 ± 0.1	1.10	Im: N—***C***(H)—N	C2
	131.7 ± 1.0	133.5 ± 7.2	0.0 ± 0.1	0.48	nIm: N—***C***H—***C***H—N	C3
	125.6 ± 1.0	129.6 ± 7.6	0.1 ± 0.1	0.64	Im: N—***C***H—***C***H—N	C3
ZIF-78	157.8 ± 1.0	100.6 ± 5.0	0.0 ± 0.1	3.49	nbIm: N—***C***(H)—N	C2
	152.1 ± 0.5	84.9 ± 5.5	−0.4 ± 0.1	1.29	nIm: N—***C***(NO_2)—N	C2
	146.0 ± 0.2	147.0 ± 6.4	0.6 ± 0.1	0.17	nbIm: C	C4/6/9
	143.5 ± 0.2	119.8 ± 8.0	0.0 ± 0.1	0.28	nbIm: C	C4/6/9
	140.8 ± 0.2	141.1 ± 7.3	−0.6 ± 0.1	0.13	nbIm: C	C4/6/9
	133.6 ± 0.5	132.9 ± 15.8	0.0 ± 0.1	2.32	nIm: N—***C***H═***C***H—N	C3
	132.4 ± 0.2	137.6 ± 9.2	0.0 ± 0.1	1.67	nIm: N—***C***H═***C***H—N	C3
	118.8 ± 0.2	165.5 ± 7.1	−0.4 ± 0.1	3.07	nbIm: CH	C5/7/8
	115.3 ± 0.2	163.2 ± 7.3	−0.3 ± 0.1	1.71	nbIm: CH	C5/7/8
	114.4 ± 0.2	152.7 ± 7.5	−0.4 ± 0.1	2.56	nbIm: CH	C5/7/8
	111.6 ± 0.2	148.5 ± 6.3	−0.5 ± 0.1	1.28	nbIm: CH	C5/7/8

Table 6
Experimental ^{15}N (9.4 T) NMR parameters (δ_{iso}, Ω, κ) and rms errors, along with the assignment of resonances observed for a range of dual-linker ZIFs.

	δ_{iso} (ppm)	Ω (ppm)	κ	rms error	Assignment	
ZIF-68	−26.9 ± 0.1[a]				nIm: C(***N***O_2)	N4
	−170.9 ± 0.1	231.8 ± 9.6	1.0 ± 0.1	3.46	nIm: ***N***—C(NO_2)—***N***	N1
	−172.9 ± 0.1	201.3 ± 11.2	1.0 ± 0.1	129.68	nIm: ***N***—C(NO_2)—***N***	N1
	−191.6 ± 0.1	189.5 ± 21.8	0.6 ± 0.3	70.39	bIm: ***N***—C(H)—***N***	N1
ZIF-70	−27.5 ± 0.2[a]				nIm: C(***N***O_2)	N4
	−175.0 ± 0.2	219.1 ± 17.4	0.5 ± 0.2	6.12	nIm/Im: ***N***	N1
ZIF-78	−10.0 ± 0.1	220.0 ± 11.0	0.2 ± 0.2	21.87	nbIm: C(***N***O_2)	N10
	−27.1 ± 0.1	210.0 ± 11.0	0.0 ± 0.2	8.93	nIm: C(***N***O_2)	N4
	−173.4 ± 0.1	237.3 ± 11.2	0.5 ± 0.2	4.50	nIm: ***N***—C(NO_2)—***N***	N1
	−184.6 ± 0.1	205.6 ± 10.5	0.4 ± 0.2	20.32	nbIm: ***N***—C(H)—***N***	N1
	−188.4 ± 0.1	200.9 ± 18.0	0.6 ± 0.2	3.59	nbIm: ***N***—C(H)—***N***	N1

[a] Signal intensity too low to extract CSA parameters accurately.

coloured according to the ZIF from which they result. The points clearly fall into separate regions, with N—***C***(X)—N species (shown by crosses) having high δ_{iso} (between 145 and 155 ppm). There is a variation in Ω (between 80 and 140 ppm), with the smallest Ω observed when R = NO_2, *i.e.*, when C2 is bonded to three N. Highest Ω are found for R = H. The N—***C***H═***C***H—N species in the Im, mIm and nIm linkers (denoted by the filled circles) have very similar δ_{iso} (125–132 ppm) and Ω (~130 ppm). For bIm-based linkers, the related, but now unprotonated, N—***C***═***C***—N species (denoted by filled and open squares) generally have higher δ_{iso} (140–145 ppm), but similar Ω. The C species in the benzene rings have the lowest δ_{iso} and the highest Ω, with the introduction of the —NO_2 group for ZIF-78 resulting in a decrease in δ_{iso} and Ω. A plot of the experimental ^{15}N δ_{iso} against Ω is shown in Fig. 6b. The N species can be clearly differentiated by their δ_{iso} values, with —***N***O_2 at much higher shifts (−25 to 0 ppm) and Im N species between −150 and −200 ppm. Unlike ^{13}C, a fairly wide range of Ω values are observed for the Im N, with little clear correlation with δ_{iso} or with the chemical nature of the linker. Owing to low sensitivity, it was not possible to measure Ω for all —***N***O_2 groups, so it is not currently possible to comment more generally on the typical Ω for these species.

4. Conclusions

In this work we have investigated the ^{13}C and ^{15}N NMR parameters of a series of ZIFs, prepared using one or more functionalised imidazolate and/or benzimidazolate linkers. In most cases, the resonances in the solid-state NMR spectra can be tentatively assigned by combining a basic knowledge of the chemical shifts observed for linker molecules in solution with dipolar dephasing experiments to identify quaternary C species. Owing to the chemical complexity of the systems studied, *i.e.*, the size of the unit cells, the presence of linker disorder, disorder in the orientation of functionalised linkers and the presence and dynamics of solvent/water molecules within the pores of the materials, it is difficult to assign resonances to specific crystallographic sites, or to use periodic DFT calculations to predict exact shifts. However, calculations performed for ordered model systems were able to aid and confirm the spectral assignment for some of the simpler ZIFs. Measurement of the anisotropic component of the shielding, specifically Ω, using amplified PASS experiments provides additional support for the spectral assignment.

The plots in Fig. 6 indicate that the ^{13}C and ^{15}N NMR parameters are sufficiently sensitive to detect small differences in chemical environments, *e.g.*, changes to topology, linker functionalisation or the presence of molecules within the pores, when comparing different ZIFs or different forms of the same ZIF. However, the magnitude of δ_{iso} and Ω observed relate primarily to the chemical nature of the linker, and so measurement of both parameters, particularly for ^{13}C, provides strong support for determining the type(s) of linkers present. For example, spectra of the dual-linker ZIFs contain resonances with very similar shifts to those of ZIFs composed of just one linker, and so the chemical nature of the C species can be determined despite considerable spectral overlap in some

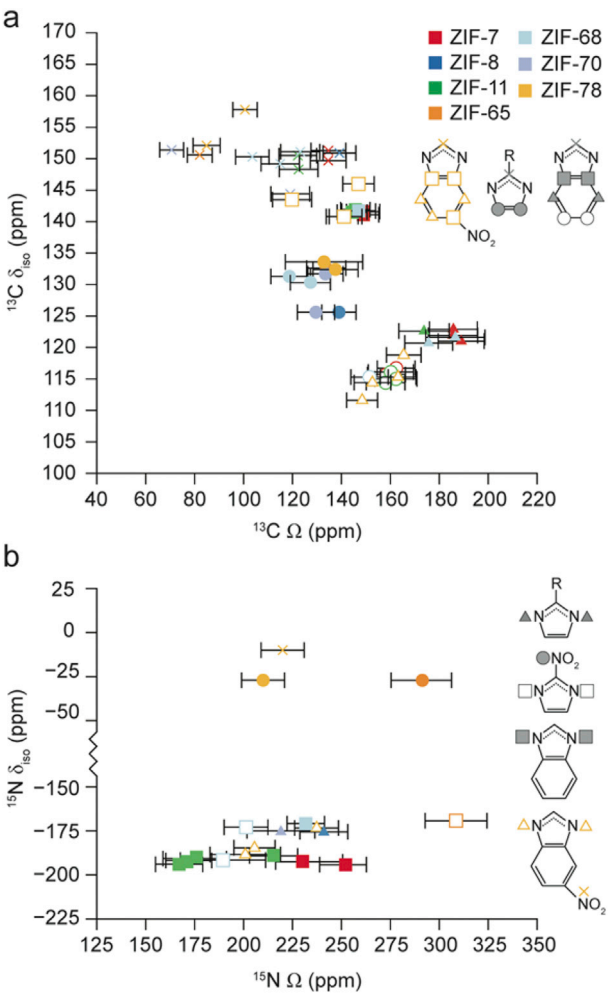

Fig. 6. Plot of (a) ^{13}C and (b) ^{15}N Ω against δ_{iso} for all single- and dual-linker ZIFs studied (with the exception of ZIF-20). Symbols denote the type of chemical species/linker, and the colour denotes the ZIF from which the points derive.

cases, demonstrating the value of this type of linker "library". For these materials, some indication of the relative proportion of each linker present can be obtained from the relative intensities of resonances from chemically-similar C species that are well-resolved in the ^{13}C CP MAS NMR spectrum, although care must be taken to ensure that the distributions of nearby H are sufficiently similar. Some progress may be made in this respect in the future by investigating the applicability of the multiple-contact CP approach,[51] to ZIFs (and MOFs more generally). This work has initiated the more general task of creating a library of NMR parameters of single- and dual-linker ZIFs that can be used not only by the solid-state NMR community, but also the wider materials chemistry community to help to understand and assign NMR spectra. The results will also be useful to help solve the structures of new (and particularly complex and disordered) ZIFs and to characterise those subjected to post-synthetic modification.

Acknowledgements

We are grateful to EPSRC computational support through the Collaborative Computational Project on NMR Crystallography (CCP-NC), via EP/M022501/1, and for other support through EP/G062129/1 (JK) and EP/M506631/1 (SS). AFO acknowledges funding from the European Community Seventh Framework Program (FP7/2007–2013 [grant agreement number 608490], Project M4CO2). SEA would also like to thank the Royal Society and Wolfson Foundation for a merit award. AFO would also like to acknowledge the SCI for a scholarship for her PhD studies. Some of the calculations were performed on the ARCHER UK National Supercomputing Service, and were supported by CCP-NC. The research data (and/or materials) supporting this publication can be accessed at http://dx.doi.org/10.17630/7959a81e-161d-4ada-9914-08d3d235ce88.

Appendix A. Supplementary data

Supplementary data related to this article can be found at http://dx.doi.org/10.1016/j.ssnmr.2017.09.001.

References

[1] K.S. Park, Z. Ni, A.P. Côté, J.Y. Choi, R. Huang, F.J. Uribe-Romo, H.K. Chae, M. O'Keeffe, O.M. Yaghi, Exceptional chemical and thermal stability of zeolitic imidazolate frameworks, Proc. Nat. Acad. Sci. U.S.A. 103 (2006) 10186–10191.
[2] A. Phan, C.J. Doonan, F.J. Uribe-Romo, C.B. Knobler, M. O'Keeffe, O.M. Yaghi, Synthesis, structure, and carbon dioxide capture properties of zeolitic imidazolate frameworks, Acc. Chem. Res. 43 (2010) 58–67.
[3] R. Banerjee, A. Phan, B. Wang, C. Knobler, H. Furukawa, M.O.' Keeffe, O.M. Yaghi, High-throughput synthesis of zeolitic imidazolate frameworks and application to CO2 capture, Science 319 (2008) 939–943.
[4] B. Chen, Z. Yang, Y. Zhu, Y. Xia, Zeolitic imidazolate framework materials: recent progress in synthesis and applications, J. Mater. Chem. A 2 (2014) 16811–16831.
[5] B.R. Pimentel, A. Parulkar, E.-K. Zhou, N.A. Brunelli, R.P. Lively, Zeolitic imidazolate frameworks: next-generation materials for energy-efficient gas separations, ChemSusChem 7 (2014) 3202–3240.
[6] B. Wang, A.P. Côté, H. Furukawa, M. O'Keeffe, O.M. Yaghi, Colossal cages in zeolitic imidazolate frameworks as selective carbon dioxide reservoirs, Nature 453 (2008) 207–211.
[7] Y.-Q. Tian, Y.-M. Zhao, Z.-X. Chen, G.-N. Zhang, L.-H. Weng, D.-Y. Zhao, Design and generation of extended zeolitic metal–organic frameworks (ZMOFs): synthesis and crystal structures of zinc(II) imidazolate polymers with zeolitic topologies, Chem. Eur. J. 13 (2007) 4146–4154.
[8] P. Horcajada, T. Chalati, C. Serre, B. Gillet, C. Sebrie, T. Baati, J.F. Eubank, D. Heurtaux, P. Clayette, C. Kreuz, J.-S. Chang, Y.K. Hwang, V. Marsaud, P.-N. Bories, L. Cynober, S. Gil, G. Férey, P. Couvreur, R. Gref, Porous metal–organic-framework nanoscale carriers as a potential platform for drug delivery and imaging, Nat. Mater 9 (2009) 172–178.
[9] J. An, S.J. Geib, N.L. Rosi, Cation-triggered drug release from a porous Zinc−Adeninate Metal−Organic framework, J. Am. Chem. Soc. 131 (2009) 8376–8377.
[10] W. Morris, C.J. Doonan, H. Furukawa, R. Banerjee, O.M. Yaghi, Crystals as molecules: postsynthesis covalent functionalization of zeolitic imidazolate frameworks, J. Am. Chem. Soc. 130 (2008) 12626–12627.
[11] R. Banerjee, H. Furukawa, D. Britt, C. Knobler, M. O'Keeffe, O.M. Yaghi, Control of pore size and functionality in isoreticular zeolitic imidazolate frameworks and their carbon dioxide selective capture properties, J. Am. Chem. Soc. 131 (2009) 3875–3877.
[12] Y. Ban, Y. Li, Y. Peng, H. Jin, W. Jiao, X. Liu, W. Yang, Metal-substituted zeolitic imidazolate framework ZIF-108: gas-sorption and membrane-separation properties, Chem. Eur. J. 20 (2014) 11402–11409.
[13] H. Fei, J.F. Cahill, K.A. Prather, S.M. Cohen, Tandem postsynthetic metal Ion and ligand exchange In zeolitic imidazolate frameworks, Inorg. Chem. 52 (2013) 4011–4016.
[14] M. Kim, J.F. Cahill, H. Fei, K.A. Prather, S.M. Cohen, Postsynthetic ligand and cation exchange in robust metal–organic frameworks, J. Am. Chem. Soc. 134 (2012) 18082–18088.
[15] S.E. Ashbrook, D.M. Dawson, J.M. Griffin, Local Structural Characterisation, John Wiley & Sons Ltd, Chichester, UK, 2014.
[16] K.J.D. MacKenzie, M.E. Smith, Multinuclear Solid-state NMR of Inorganic Materials, Pergamon Press, Oxford, UK, 2002.
[17] S.E. Ashbrook, D.M. Dawson, V.R. Seymour, Recent developments in solid-state NMR spectroscopy of crystalline microporous materials, Phys. Chem. Chem. Phys. 16 (2014) 8223–8242.
[18] A. Sutrisno, Y. Huang, Solid-state NMR: a powerful tool for characterization of metal–organic frameworks, Solid State Nucl. Magn. Reson 49–50 (2013) 1–11.
[19] A. Sutrisno, L. Liu, J. Xu, Y. Huang, Natural abundance solid-state ^{67}Zn NMR characterization of microporous zinc phosphites and zinc phosphates at ultrahigh magnetic field, Phys. Chem. Chem. Phys. 13 (2011) 16606–16617.
[20] A. Sutrisno, V.V. Terskikh, Q. Shi, Z. Song, J. Dong, S.Y. Ding, W. Wang, B.R. Provost, T.D. Daff, T.K. Woo, Y. Huang, Characterization of Zn-Containing metal–organic frameworks by solid-state ^{67}Zn NMR spectroscopy and computational modeling, Chem. Eur. J. 18 (2012) 12251–12259.
[21] P. He, B.E.G. Lucier, V.V. Terskikh, Q. Shi, J. Dong, Y. Chu, A. Zheng, A. Sutrisno, Y. Huang, Spies within metal-organic frameworks: investigating metal centers using solid-state NMR, J. Phys. Chem. C 118 (2014) 23728–23744.
[22] S.E. Ashbrook, S. Sneddon, New methods and applications in solid-state NMR spectroscopy of quadrupolar nuclei, J. Am. Chem. Soc. 136 (2014) 15440–15456.
[23] R.F. Moran, D.M. Dawson, S.E. Ashbrook, Exploiting NMR spectroscopy for the study of disorder in solids, Int. Rev. Phys. Chem. 36 (2017) 39–115.
[24] C. Bonhomme, C. Gervais, F. Babonneau, C. Coelho, F. Pourpoint, T. Azaïs, S.E. Ashbrook, J.M. Griffin, J.R. Yates, F. Mauri, C.J. Pickard, First-principles

calculation of NMR parameters using the gauge including projector augmented wave method: a Chemist's point of view, Chem. Rev. 112 (2012) 5733–5779.
[25] S.E. Ashbrook, D. McKay, Combining solid-state NMR spectroscopy with first principles calculations – a guide to NMR Crystallography, Chem. Commun. 52 (2016) 7186–7204.
[26] O.N. Antzutkin, Sideband manipulation in magic-angle-spinning nuclear magnetic resonance, Prog. Nucl. Magn. Reson. Spectrosc. 35 (1999) 203–266.
[27] L. Shao, J.J. Titman, Chemical shift anisotropy amplification, Prog. Nucl. Magn. Reson. Spectrosc. 51 (2007) 103–137.
[28] R.M. Orr, M.J. Duer, Applications of the CSA-amplified PASS experiment, Solid State Nucl. Magn. Reson 30 (2006) 1–8.
[29] R.M. Orr, M.J. Duer, S.E. Ashbrook, Correlating fast and slow chemical shift spinning sideband patterns in solid-state NMR, J. Magn. Reson 174 (2005) 301–309.
[30] M.R. Mitchell, D. Carnevale, R. Orr, K.R. Whittle, S.E. Ashbrook, Exploiting the chemical shielding anisotropy to probe structure and disorder in ceramics: ^{89}Y MAS NMR and first-principles calculations, J. Phys. Chem. C 116 (2012) 4273–4286.
[31] D. Carnevale, S.E. Ashbrook, G. Bodenhausen, Solid-state NMR measurements and DFT calculations of the magnetic shielding tensors of protons of water trapped in barium chlorate monohydrate, RSC Adv. 4 (2014) 56248–56258.
[32] S.E. Ashbrook, M.R. Mitchell, S. Sneddon, R.F. Moran, M. de los Reyes, G.R. Lumpkin, K.R. Whittle, New insights into phase distribution, phase composition and disorder in $Y_2(Zr,Sn)_2O_7$ ceramics from NMR spectroscopy, Phys. Chem. Chem. Phys. 17 (2015) 9049–9059.
[33] S. Sneddon, University of St Andrews, PhD Thesis, 2016.
[34] E.F. Baxter, T.D. Bennett, C. Mellot-Draznieks, C. Gervais, F. Blanc, A.K. Cheetham, Combined experimental and computational NMR study of crystalline and amorphous zeolitic imidazolate frameworks, Phys. Chem. Chem. Phys. 17 (2005) 25191–25196.
[35] X. Huang, J. Zhang, X. Chen, $[Zn(bim)_2] \cdot (H_2O)_{1.67}$: a metal-organic open-framework with sodalite topology, Chin. Sci. Bull. 48 (2003) 1531–1534.
[36] H. Hayashi, A.P. Côté, H. Furukawa, M. O'Keeffe, O.M. Yaghi, Zeolite a imidazolate frameworks, Nat. Mater 6 (2007) 501–506.
[37] A.E. Bennett, C.M. Rienstra, M. Auger, K.V. Lakshmi, R.G. Griffin, Heteronuclear decoupling in rotating solids, J. Chem. Phys. 103 (1995) 6951–6958.
[38] D. Sandström, M.H. Levitt, Structure, Molecular, Ordering of a nematic liquid crystal studied by natural-abundance double-quantum ^{13}C NMR, J. Am. Chem. Soc. 118 (1996) 6966–6974.
[39] M.H. Levitt, P.K. Madhu, C.E. Hughes, Cogwheel phase cycling, J. Magn. Reson 155 (2002) 300–306.
[40] M. Bak, J.T. Rasmussen, N.C. Nielsen, SIMPSON: a general simulation Program for solid-state NMR spectroscopy, J. Magn. Reson 147 (2000) 296–330.
[41] J. Herzfeld, A.E. Berger, Sideband intensities in NMR spectra of samples spinning at the magic angle, J. Chem. Phys. 73 (1980) 6021–6030.
[42] R.K. Harris, E.D. Becker, S.M.C. de Menezes, P. Granger, R.E. Hoffman, K.W. Zilm, Further conventions for NMR shielding and chemical shifts (IUPAC recommendations 2008), Pure Appl. Chem. 80 (2008) 59–84.
[43] M.D. Segall, P.J.D. Lindan, M.J. Probert, C.J. Pickard, P.J. Hasnip, S.J. Clark, M.C. Payne, First-principles simulation: ideas, illustrations and the CASTEP code, J. Phys. Condens. Matter 14 (2002) 2717–2744.
[44] C.J. Pickard, F. Mauri, All-electron magnetic response with pseudopotentials: NMR chemical shifts, Phys. Rev. B 63 (2001) 245101.
[45] J.P. Perdew, K. Burke, M. Ernzerhof, Generalized gradient approximation made simple, Phys. Rev. Lett. 77 (1996) 3865–3868.
[46] J.R. Yates, C.J. Pickard, F. Mauri, Calculation of NMR chemical shifts for extended systems using ultrasoft pseudopotentials, Phys. Rev. B 76 (2007) 024401.
[47] E.R. McNellis, J. Meyer, K. Reuter, Azobenzene at Coinage Metal Surfaces: role of Dispersive van der Waals Interactions, Phys. Rev. B 80 (2009) 205414.
[48] A. Tkatchenko, M. Scheffler, Accurate Molecular van der Waals Interactions from Ground-State Electron Density and Free-Atom Reference Data, Phys. Rev. Lett. 102 (2009) 073005.
[49] A. Orsi, D.J. Price, J. Kahr, R.S. Pillai, S. Sneddon, S. Cao, V. Benoit, M.M. Łozińska, D.B. Cordes, A.M.Z. Slawin, P.L. Llewellyn, I. Casely, S.E. Ashbrook, G. Maurin, P.A. Wright, Porous zinc and cobalt 2-nitroimidazolate frameworks with six-membered ring windows and a layered cobalt 2-nitroimidazolate polymorph, CrystEngComm 19 (2017) 1377–1388.
[50] Z. Han, A.L. Picone, A.M.Z. Slawin, V.R. Seymour, S.E. Ashbrook, W. Zhou, S.P. Thompson, J.E. Parker, P.A. Wright, Novel large-pore aluminophosphate molecular sieve STA-15 prepared using the tetrapropylammonium cation as a structure directing agent, Chem. Mater 22 (2010) 338–346.
[51] R.L. Johnson, K. Schmidt-Rohr, Quantitative solid-state ^{13}C NMR with signal enhancement by multiple cross polarization, J. Magn. Reson 239 (2014) 44–49.